CrystEngComm

PAPER

View Article Online
View Journal

Cite this: DOI: 10.1039/d5ce01151e

Structure-directing roles of polycarboxylate anions in the formation of Ag(I) coordination polymers with mixed ligands

Yi-Lin Shen, Chia-Li Liu, Hsun-Chih Tai, Zhi-Ling Chen and Jhy-Der Chen *

Received 6th December 2025, Accepted 26th January 2026

DOI: 10.1039/d5ce01151e

rsc.li/crystengcomm

Hydrothermal reactions of bis-pyridyl-bis-amide with polycarboxylic acid and Ag(I) salt afforded $\{[Ag(\mathbf{L^1})][HCDDC]\}_n$ [$\mathbf{L^1}$ = *N,N'*-di(4-methylpyridyl)oxamide; H_2CDDC = 7-carboxy-1,3-dioxo-1,3-dihydrobenzo[*de*]isochromene-6-carboxylic acid], **1**, $\{[Ag(\mathbf{L^1})][1,4\text{-}HNDC]\cdot 2H_2O\}_n$ (1,4-H_2NDC = 1,4-naphthalenedicarboxylic acid), **2**, $[Ag(1,2,4,5\text{-}H_2BTEC)_{0.5}(\mathbf{L^1})_{0.5}]_n$ (1,2,4,5-H_4BTC = 1,2,4,5-benzenetetracarboxylic acid), **3**, $\{[Ag(\mathbf{L^1})(H_2O)][1,2,4,5\text{-}H_3CTC]\cdot H_2O\}_n$ (1,2,4,5-H_4CTC = 1,2,4,5-cyclohexanetetracarboxylic acid), **4**, $\{[Ag(\mathbf{L^2})][1,4\text{-}HNDC]\cdot H_2O\}_n$ [$\mathbf{L^2}$ = *N,N'*-di(3-pyridyl)oxamide; 1,4-H_2NDC = 1,4-naphthalenedicarboxylic acid], **5**, $\{[Ag_2(\mathbf{L^1})_2][1,2,4\text{-}HBTC]\cdot 2H_2O\}_n$ (1,2,4-H_3BTC = 1,2,4-benzenetricarboxylic acid), **6**, $\{[Ag_2(\mathbf{L^1})_{1.5}][(1,3,5\text{-}HBTC)(H_2O)]\cdot 2H_2O\}_n$ (1,3,5-H_3BTC = 1,3,5-benzenetricarboxylic acid), **7**, $\{[Ag(\mathbf{L^1})_{0.5}][(1,3,5\text{-}H_2BTC)]\}_n$, **8**, and $\{[Ag_5(1,3,5\text{-}HBTC)(1,3,5\text{-}BTC)(\mathbf{L^1})_2]\cdot 5H_2O\}_n$, **9**, which have been structurally identified by using single-crystal X-ray diffraction. Complexes **1**, **2**, **4**, **5** and **6** are 1D zigzag chains and **8** forms a 1D looped chain, whereas **3** features a 3D framework with the **fsh** topology, **7** reveals a linear tetranuclear molecule and **9** adopts a 3-fold interpenetrated 3D framework with the **sra** topology. The roles of the polycarboxylate anions in determining the structural diversity of these Ag(I) complexes are evaluated.

Introduction

The rational design and synthesis of novel coordination polymers (CPs) have become an active area of investigation because such that the range of these crystalline functional materials with pre-selected physical and chemical properties can be further expanded.[1–11] The varieties of the CPs that can be approached rely on the presence of suitable metal–ligand interactions and supramolecular contacts, *i.e.*, hydrogen bonds and other weak interactions. The properties of CPs are mostly dominated by their structures and compositions and it is well known that the structural type of CPs is determined by several factors such as the identities of metal ions, counter ions and organic linkers.[12–15] Therefore, controlling the appropriate factors to construct suitable CPs have become an exciting topic in the crystal engineering of CPs. On the other hand, Ag(I) CPs have attracted great attention due to their structural variability and extensive industrial and medical applications.[16–24]

While many Ag(I) CPs with mixed ligands involving dipyridyl and polycarboxylate ligands have been reported, the coordination of the polycarboxylate ligands to Ag(I) ions remain unjustified, presumably due to the hard base character of the polycarboxylate ligands and the soft acid character of the Ag(I) ion. Short Ag⋯Ag and Ag⋯O distances were observed in the structurally characterized complexes with bridging ligands (ligand-supported) and the attractive phenomenon of Ag⋯Ag interactions was generally accepted after examples of ligand-unsupported ones were reported.[25] The Ag⋯Ag distance is generally longer than that of the metallic Ag⋯Ag contact (2.89 Å), but shorter than the van der Waals contact distance (3.40 A°), whereas the Ag⋯O distances are longer than the upper limit of 2.3–2.6 Å for Ag–O bonds,[26] but are significantly shorter than the corresponding van der Waals contacts of Ag and O atoms which is 3.24 Å (van der Waals radii for Ag = 1.72 and O = 1.52 Å).[27] The Ag⋯O distances to the polycarboxylate anions are thus important in determining the structural topologies of the Ag(I) CPs thus prepared and should be carefully evaluated.

With this background information, we sought to investigate the roles of the polycarboxylate ligands in determining the structural diversity of the bis-pyridyl-bis-amide (bpba)-based Ag(I) CPs. Herein, we report the syntheses and structures of $\{[Ag(\mathbf{L^1})][HCDDC]\}_n$ [$\mathbf{L^1}$ = *N,N'*-di(4-methylpyridyl)oxamide; H_2-CDDC = 7-carboxy-1,3-dioxo-1,3-dihydrobenzo[*de*]isochromene-6-carboxylic acid], **1**, $\{[Ag(\mathbf{L^1})][1,4\text{-}HNDC]\cdot 2H_2O\}_n$ (1,4-H_2NDC = 1,4-naphthalenedicarboxylic acid), **2**, $[Ag(1,2,4,5\text{-}H_2\text{-}BTEC)_{0.5}(\mathbf{L^1})_{0.5}]_n$ (1,2,4,5-H_4BTC = 1,2,4,5-benzenetetracarboxylic acid), **3**, $\{[Ag(\mathbf{L^1})(H_2O)][1,2,4,5\text{-}H_3CTC]\cdot H_2O\}_n$ (1,2,4,5-H_4CTC = 1,2,4,5-cyclohexanetetracarboxylic acid), **4**, $\{[Ag(\mathbf{L^2})][1,4\text{-}$

Department of Chemistry, Chung Yuan Christian University, Chung-Li, Taiwan, R.O.C. E-mail: jdchen@cycu.edu.tw

HNDC]·H_2O}$_n$ [$\mathbf{L^2}$ = *N*,*N*′-di(3-pyridyl)oxamide; 1,4-H_2NDC = 1,4-naphthalenedicarboxylic acid], **5**, {[$Ag_2(\mathbf{L^1})_2$][1,2,4-HBTC]·$2H_2O$}$_n$ (1,2,4-H_3BTC = 1,2,4-benzenetricarboxylic acid), **6**, {[$Ag_2(\mathbf{L^1})_{1.5}$][(1,3,5-HBTC)(H_2O)]·$2H_2O$}$_n$ (1,3,5-H_3BTC = 1,3,5-benzenetricarboxylic acid), **7**, {[$Ag(\mathbf{L^1})_{0.5}$][(1,3,5-H_2BTC)]}$_n$, **8**, and {[Ag_5(1,3,5-HBTC)(1,3,5-BTC)$(\mathbf{L^1})_2$]·$5H_2O$}$_n$, **9**. The roles of the Ag⋯Ag and Ag⋯O interactions in determining the topological structures of these CPs are discussed. Fig. 1 depicts the structures of $\mathbf{L^1}$ and $\mathbf{L^2}$ and Fig. 2 shows the structures of the polycarboxylic acids, respectively.

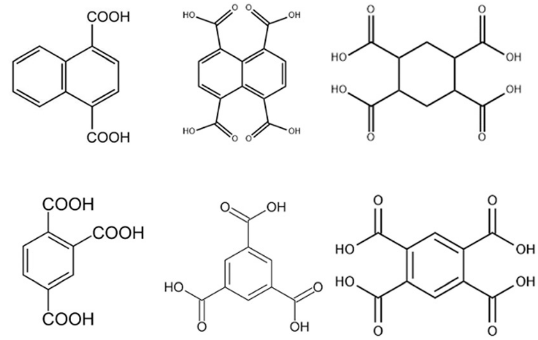

Fig. 2 From left to right, first row: structures of 1,4-H_2NDC, 1,4,5,8-H_4NTC and 1,2,4,5-H_4CTC. Second row: 1,2,4-H_3BTC, 1,3,5-H_3BTC and 1,2,4,5-H_4BTC.

Experimental details

General procedures

IR spectra (KBr disk) were obtained from a JASCO FT/IR-4200 FT-IR spectrometer. Elemental analyses were performed on an Elementar vario EL III analyzer. Powder X-ray diffraction was carried out on a Bruker D2 PHASER diffractometer with a CuK_α (λ_α = 1.54 Å) radiation.

Materials

The reagents 1,4-H_2NDC, 1,2,4-H_3BTC, and 1,3,5-H_3BTC were purchased from Alfa Aesar and 1,2,4,5-H_4CTC and 1,4,5,8-H_4NTC from NOVA. Silver acetate was obtained from ACROS. The ligands *N*,*N*′-di(4-methylpyridyl)oxamide ($\mathbf{L^1}$) and *N*,*N*′-di(3-pyridyl)oxamide ($\mathbf{L^2}$) were prepared according to published procedures.[28]

Preparation of {[$Ag(\mathbf{L^1})$][HCCDC]}$_n$, 1. A mixture of $Ag(CH_3COO)\cdot H_2O$ (0.017 g, 0.10 mmol), $\mathbf{L^1}$ (0.027 g, 0.10 mmol) and 1,4,5,8-H_4NTC (0.030 g, 0.10 mmol) in 10 mL of H_2O was sealed in a 23 mL Teflon-lined steel autoclave, which was heated under autogenous pressure to 80 °C for two days, and then cooled down to room temperature for two days. Colorless crystals suitable for single-crystal X-ray diffraction were obtained. Yield: 0.023 g (26%). Anal. calcd for $C_{26}H_{25}N_4O_8Ag$ (MW = 663.34): C, 50.69; H, 2.89; N, 8.45%. Found: C, 50.43; H, 2.83; N, 8.79%. FT-IR (cm^{-1}): 3440(s), 3180(m), 3111(w), 3013(s), 2967(m), 2876(m), 2814(s), 2789(s), 2745(s), 2681(m), 2622(m), 1131(s), 844(s).

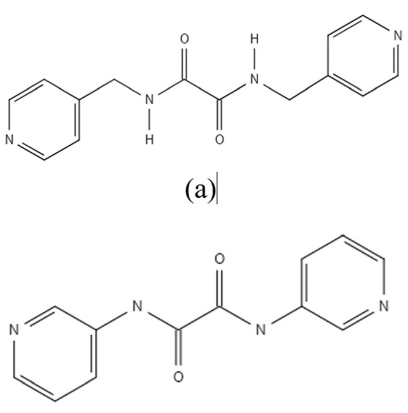

(a) (b)

Fig. 1 Structures of (a) $\mathbf{L^1}$ and (b) $\mathbf{L^2}$.

Preparation of {[$Ag(\mathbf{L^1})$][1,4-HNDC]·$2H_2O$}$_n$, 2. Complex **2** was prepared by following similar procedures to **1**, except that $Ag(CH_3COO)\cdot H_2O$ (0.017 g, 0.10 mmol), $\mathbf{L^1}$ (0.027 g, 0.10 mmol) and 1,4-H_2NDC (0.022 g, 0.010 mmol) were used. Colorless crystals were obtained. Yield: 0.041 g (65%). Anal. calcd for $C_{26}H_{25}N_4O_8Ag$ (MW = 629.37): C, 49.62; H, 4.00; N, 8.90%. Found: C, 49.68; H, 3.65; N, 9.16%. FT-IR (cm^{-1}): 3440(s), 3783(w), 3608(m), 3330(w), 3203(w), 3127(w), 2979(m), 2878(s), 2796(s), 2713(s), 2037(m), 1046(s), 916(s).

Preparation of [Ag(1,2,4,5-H_2BTEC)$_{0.5}$$(\mathbf{L^1})_{0.5}$]$_n$, 3. Complex **3** was prepared by following similar procedures to **1**, except that $Ag(CH_3COO)\cdot H_2O$ (0.017 g, 0.10 mmol), $\mathbf{L^1}$ (0.027 g, 0.10 mmol) and 1,2,4,5-H_4BTEC (0.0210 g, 0.10 mmol) were used. Colorless crystals were obtained. Yield: 0.026 g (70%). Anal. calcd for $C_{12}H_9N_2O_5Ag$ (MW = 369.08): C, 39.05; H, 2.46; N, 7.59%. Found: C, 39.32; H, 2.21; N, 7.98%. FT-IR (cm^{-1}): 3914(m), 3884(w), 3786(m), 3641(w), 3590(w), 3258(w), 3048(m), 3015(m), 2816(s), 2744(s), 2054(w), 1127(s), 953(s).

Preparation of {[$Ag(\mathbf{L^1})(H_2O)$][1,2,4,5-H_3CHTC]·H_2O}$_n$, 4. Complex **4** was prepared by following similar procedures to **1**, except that $Ag(CH_3COO)\cdot H_2O$ (0.017 g, 0.10 mmol), $\mathbf{L^1}$ (0.027 g, 0.10 mmol) and 1,4,5,8-H_4CHTC (0.0210 g, 0.10 mmol) were used. Colorless crystals were obtained. Yield: 0.0261 g (39%). Anal. calcd for $C_{24}H_{19}N_4O_7Ag$ (MW = 673.38): C, 42.80; H, 4.34; N, 8.32%. Found: C, 42.45; H, 3.95; N, 8.56%. FT-IR (cm^{-1}): 3926(m), 3781(m), 3608(m), 3126(m), 2978(s), 2883(s), 2794(s), 2714(s), 1582(w), 1333(m), 1132(s), 1042(s), 917(s).

Preparation of {[$Ag(\mathbf{L^2})$][1,4-HNDC]·H_2O}$_n$, 5. Complex **5** was prepared by following similar procedures to **1**, except that $Ag(CH_3COO)\cdot H_2O$ (0.017 g, 0.10 mmol), $\mathbf{L^2}$ (0.025 g, 0.1 mmol) and 1,4-H_2NDC (0.022 g, 0.10 mmol) were used. Colorless crystals were obtained. Yield: 0.012 g (20%). Anal. calcd for $C_{24}H_{19}N_4O_7Ag$ (MW = 583.30): C, 49.42; H, 3.28; N, 9.60%. Found: C, 49.35; H, 2.98; N, 9.89%. FT-IR (cm^{-1}): 3702(w), 3591(w), 3204(w), 3131(w), 3048(m), 2978(m), 2871(m), 2814(s), 2744(m), 2715(m), 2029(w), 1131(s), 969(s).

Preparation of{[$Ag_2(\mathbf{L^1})_2$](1,2,4-HBTC)·$2H_2O$}$_n$, 6. Complex **6** was prepared by following similar procedures to **1**, except that $Ag(CH_3COO)\cdot H_2O$ (0.017 g, 0.10 mmol), $\mathbf{L^1}$ (0.027 g, 0.1 mmol) and 1,2,4-H_3BTC (0.021 g, 0.10 mmol) were used. Colorless crystals suitable for single-crystal X-ray diffraction were obtained. Yield: 0.018 g (18%). Anal. calcd for $C_{37}H_{36}N_8O_{12}Ag_2$ (MW = 1000.46): C, 44.42; H, 3.63; N, 11.20%. Anal. calcd for $C_{37}H_{36}N_8O_{12}Ag_2 - 2H_2O$ (MW = 964.45): C, 46.08; H, 3.34; N, 11.62%. Found: C, 46.94; H, 3.09; N, 11.50%. FT-IR (cm^{-1}): 3432(s), 2813(w), 2724(w), 1587(s), 1380(m), 1345(m), 761(m), 613(m).

Preparation of $\{[Ag_2(L^1)_{1.5}][(1,3,5\text{-}HBTC)(H_2O)]\cdot 2H_2O\}_n$, 7. Complex **7** was prepared by following similar procedures to **1**, except that $Ag(CH_3COO)\cdot H_2O$ (0.017 g, 0.10 mmol), $\mathbf{L^1}$ (0.027 g, 0.10 mmol) and 1,3,5-H_3BTC (0.021 g, 0.10 mmol) were used. Colorless crystals were obtained. Yield: 0.028 g (31%). Anal. calcd for $C_{30}H_{31}N_6O_{12}Ag_2$ (MW = 883.34): C, 40.79; H, 3.54; N, 9.51%. Found: C, 41.54; H, 3.22; N, 9.55%. Anal. calcd for $C_{30}H_{31}N_6O_{12}Ag_2 - 1H_2O$ (MW = 865.32): C, 41.64; H, 3.38; N, 9.71%. Found: C, 41.65; H, 3.21; N, 9.85%. FT-IR (cm^{-1}):3434(s), 2811(w), 2728(w), 2364(w), 1586(s), 1379(m), 1347(m), 760(m), 670(m), 615(m).

Preparation of $\{[Ag(L^1)_{0.5}][(1,3,5\text{-}H_2BTC)]\}_n$, 8. Complex **8** was prepared by following similar procedures to **1**, except that $Ag(CH_3COO)\cdot H_2O$ (0.050 g, 0.30 mmol), $\mathbf{L^1}$ (0.027 g, 0.10 mmol) and 1,3,5-H_3BTC (0.063 g, 0.30 mmol) were used. Colorless crystals were obtained. Yield: 0.057 g (42%). Anal. calcd for $C_{16}H_{12}N_2O_7Ag$ (MW = 452.15): C, 42.50; H, 2.68; N, 6.20%. Found: C, 42.53; H, 2.62; N, 6.56%. FT-IR (cm^{-1}): 3444(s), 2815(w), 2726(w), 2371(w), 1589(s), 1384(m), 1346(m), 1123(w), 763(m), 612(m). There are some minor crystals that can be structurally characterized as $\{[Ag_5(1,3,5\text{-}HBTC)(1,3,5\text{-}BTC)(\mathbf{L^1})_2]\cdot 5H_2O\}_n$, **9**. Yield: less than 1%. FT-IR (cm^{-1}): 3436(s), 2892(m), 1605(m), 1501(m), 1332(m), 1133(s), 1046(s), 921(m).

X-ray crystallography

The diffraction data for complexes **1–9** were collected on a Bruker AXS SMART APEX II CCD diffractometer, which was equipped with a graphite-monochromated Mo K_α (λ_α = 0.71073 Å) radiation. Data reduction was carried out by standard methods with the use of well-established computational procedures.[29] The structure factors were obtained after Lorentz and polarization corrections. An empirical absorption correction based on "multi-scan" was applied to the data. The positions of some of the heavier atoms were located by the direct or Patterson method. The remaining atoms were found in a series of alternating difference Fourier maps and least-squares refinements, while the hydrogen atoms except those of the water molecules were added by using the HADD command in SHELXTL 6.1012.[30] Table 1 lists the crystal data for **1–9**. ORTEP drawings for the crystal structures are given in the SI (Fig. S1–S9).

Results and discussion

Structure of $\{[Ag(L^1)][HCCDC]\}_n$, 1

Single-crystal X-ray diffraction analysis shows that complex **1** crystallizes in the triclinic space group $P\bar{1}$. The asymmetric unit consists of two halves of a Ag(I) cation, one $\mathbf{L^1}$ ligand and one $HCDDC^-$ anion (H_2CDDC = 7-carboxy-1,3-dioxo-1,3-dihydrobenzo[*de*]isochromene-6-carboxylate). The two independent Ag(I) cations are two-coordinated by two pyridyl nitrogen atoms from two $\mathbf{L^1}$ ligands [Ag–N = 2.149(4) and 2.114(5) Å], resulting in linear geometries (∠N–Ag–N = 180°) (Fig. 3(a)). The Ag(I) cations are linked together by $\mathbf{L^1}$ ligands to afford 1D zigzag chains (Fig. 3(b)), and the chains are further interlinked through Ag⋯O interactions [2.895(3) and 3.216(4) Å] to the $HCDDC^-$ anions to form pairs of double chains (Fig. 3(c)). The double chains are also supported by the self-complementary N–H⋯O hydrogen bonds [O⋯H = 2.151(4) Å; ∠N–H⋯O = 137.8(3)°] to the amide oxygen atoms of the adjacent chains. Transformation of the organic compound from 1,4,5,8-H_4NTC to $HCDDC^-$ is observed.

Structure of $\{[Ag(L^1)][1,4\text{-}HNDC]\cdot 2H_2O\}_n$, 2

Complex **2** crystallizes in the triclinic space group $P\bar{1}$ and each asymmetric unit consists of one Ag(I) cation, one $\mathbf{L^1}$ ligand, one 1,4-$HNDC^-$ anion and two co-crystallized water molecules. The Ag(I) cations are two-coordinated by two pyridyl nitrogen atoms from two $\mathbf{L^1}$ ligands [Ag–N = 2.176(3) and 2.182(3) Å], resulting in a distorted linear geometry [∠N–Ag–N = 163.94(12)°] (Fig. 4(a)). The Ag(I) cations are linked together by $\mathbf{L^1}$ ligands to afford a 1D zigzag chain (Fig. 4(b)), which is further interlinked by an adjacent chain through the Ag⋯Ag [3.4832(8) Å] and Ag⋯O interactions [2.616(3) and 2.662(4) Å] to the 1,4-$HNDC^-$ anions to form a double chain (Fig. 4(c)). The double chains are further extended through the O–H⋯O [O⋯H = 1.651(3) Å; ∠O–H⋯O = 164.0(2)°] hydrogen bonds between two adjacent 1,4-$HNDC^-$ anions to form a 2D layer. The 2D layers are supported by the O–H⋯O hydrogen bonds from the water molecules to the carboxylate oxygen atoms [O⋯H = 2.132(3) Å; ∠O–H⋯O = 170.3(2)°], the amide oxygen atoms [O⋯H = 1.972(3) Å; ∠O–H⋯O = 169.5(2)°] and water oxygen atoms [O⋯H = 1.984(3) and 2.051(3) Å; ∠O–H⋯ O = 170.0(2) and 151.8(2)°].

Structure of $[Ag(1,2,4,5\text{-}H_2BTEC)_{0.5}(L^1)_{0.5}]_n$, 3

The structure of complex **3** was solved in the monoclinic space group $P2_1/n$. The asymmetric unit consists of one Ag(I) cation, a half of an $\mathbf{L^1}$ ligand, and a half of a 1,2,4,5-H_2BTC^{2-} ligand. Each of the Ag(I) cations is two-coordinated by one pyridyl nitrogen atom from the $\mathbf{L^1}$ ligands [Ag–N = 2.178(4) Å] and one oxygen atom from the 1,2,4,5-H_2BTC^{2-} ligand [Ag–O = 2.218(3) Å], resulting in a distorted linear geometry [∠N–Ag–O = 164.46(14)°] (Fig. 5(a)). The Ag(I) cations are also coordinated by two amide oxygen atoms from two $\mathbf{L^1}$ ligands [Ag⋯O = 2.536(3) and 2.597(3) Å]. If the two oxygen atoms are considered to be involved in the coordination environment, the Ag(I) cation adopts a drastically distorted tetrahedral geometry. Moreover, adjacent Ag(I) ions are linked by Ag⋯Ag [3.4763(7) Å] to form a dinuclear unit (Fig. 5(b)). Considering the two Ag⋯O interactions with distances of 2.536(3) and 2.597(3) Å as coordinated covalent bonds, and

Table 1 Crystallographic data for **1–9**

CP/complex	**1**	**2**	**3**	**4**	**5**	**6**	**7**	**8**	**9**
Formula	$C_{28}H_{19}AgN_4O_9$	$C_{26}H_{25}AgN_4O_8$	$C_{12}H_9AgN_2O_5$	$C_{24}H_{29}AgN_4O_{12}$	$C_{24}H_{19}AgN_4O_7$	$C_{37}H_{36}Ag_2N_8O_{12}$	$C_{30}H_{31}Ag_2N_6O_{12}$	$C_{16}H_{12}AgN_2O_7$	$C_{46}H_{45}Ag_5N_8O_{21}$
Formula weight	663.34	629.37	369.08	673.38	583.30	1000.48	883.35	452.15	1585.25
Temperature, K	296(2)	293(2)	293(2)	293(2)	296(2)	293(2)	293(2)	293(2)	293(2)
Crystal system	Triclinic	Triclinic	Monoclinic	Monoclinic	Monoclinic	Triclinic	Triclinic	Triclinic	Triclinic
Space group	$P\bar{1}$	$P\bar{1}$	$P2_1/n$	$P2_1/c$	$P2_1/n$	$P\bar{1}$	$P\bar{1}$	$P\bar{1}$	$P\bar{1}$
a, Å	9.4392(8)	9.096(2)	12.779(2)	11.277(2)	8.5629(16)	9.4624(19)	10.8579(15)	8.6861(19)	9.627(6)
b, Å	10.4331(9)	9.557(2)	7.1294(14)	11.398(2)	25.199(5)	11.7312(19)	12.1551(15)	8.914(2)	10.094(7)
c, Å	14.5148(13)	15.651(4)	13.218(2)	21.089(4)	10.864(2)	19.160(3)	13.0789(16)	11.391(3)	31.171(18)
α, °	76.969(2)	76.424(8)	90	90	90	95.359(6)	78.820(4)	84.881(7)	85.529(16)
β, °	85.423(2)	80.583(8)	93.331(4)	91.707(5)	93.170(6)	95.325(7)	85.334(5)	70.317(5)	85.355(17)
γ, °	66.140(2)	84.483(8)	90	90	90	106.993	78.078(5)	70.793(5)	63.937(16)
V, Å^3	1273.48(19)	1302.3(6)	1202.2(4)	2709.5(9)	2340.6(8)	2008.9(6)	1655.3(4)	784.0(3)	2709(3)
Z	2	2	4	4	4	2	2	2	2
D_{calc}, mg m^{-3}	1.730	1.605	2.039	1.651	1.655	1.654	1.772	1.915	1.943
F(000)	668	640	728	1376	1176	1008	886	450	1560
μ(Mo K$_\alpha$), mm^{-1}	0.858	0.831	1.699	0.815	0.915	1.047	1.256	1.331	1.860
Range (2θ) for data collection, °	2.88–51.98	2.70–52.00	4.31–56.77	3.61–56.88	3.23–52.00	2.15–52.00	3.17–52.00	3.79–56.74	2.62–56.45
Independent reflections	5009 [R(int) = 0.0790]	5111 [R(int) = 0.0837]	2981 [R(int) = 0.0383]	6787 [R(int) = 0.0272]	4616 [R(int) = 0.0805]	7913 [R(int) = 0.1393]	6483 [R(int) = 0.0708]	3905 [R(int) = 0.0455]	13 236 [R(int) = 0.0249]
Data/restraints/parameters	5009/0/386	5111/0/352	2981/0/182	6787/0/370	4616/0/325	7913/0/542	6483/0/451	3905/0/236	13 236/0/752
Quality-of-fit indicator[c]	1.010	1.052	1.163	1.048	1.020	1.003	1.053	1.071	1.072
Final R indices [$I > 2\sigma(I)$][a,b]	R_1 = 0.0592, wR_2 = 0.1095	R_1 = 0.0440, wR_2 = 0.1037	R_1 = 0.0415, wR_2 = 0.1077	R_1 = 0.0306, wR_2 = 0.0819	R_1 = 0.0367, wR_2 = 0.0618	R_1 = 0.0596, wR_2 = 0.1241	R_1 = 0.0591, wR_2 = 0.1201	R_1 = 0.0305, wR_2 = 0.0767	R_1 = 0.0364, wR_2 =0.0949
R indices (all data)	R_1 = 0.1253, wR_2 = 0.1325	R_1 = 0.0669, wR_2 = 0.1150	R_1 = 0.0441, wR_2 = 0.1087	R_1 = 0.0353, wR_2 = 0.0849	R_1 = 0.0701, wR_2 = 0.0699	R_1 = 0.1473, wR_2 = 0.1557	R_1 = 0.0974, wR_2 = 0.1446	R_1 = 0.0344, wR_2 = 0.0792	R_1 = 0.0432, wR_2 = 0.0984

[a] $R_1 = \sum||F_o| - |F_c||/\sum|F_o|$. [b] $wR_2 = [\sum w(F_o^2 - F_c^2)^2/\sum w(F_o^2)^2]^{1/2}$. $w = 1/[\sigma^2(F_o^2) + (ap)^2 + (bp)]$, $p = [\max(F_o^2 \text{ or } 0) + 2(F_c^2)]/3$. a = 0.0391, b = 3.1802 for **1**; a = 0.0478, b = 0.39 for **2**; a = 0.0193, b = 7.5031 for **3**; a = 0.0407, b = 1.4676 for **4**; a = 0.0256, b = 1.0625 for **5**; a = 0.0538, b = 0 for **6**; a = 0.0376, b = 8.4310 for **7**; a = 0.0353, b = 0.5672 for **8**; a = 0.0428, b = 4.4862 for **9**. [c] Quality-of-fit = $[\sum w(|F_o^2| - |F_c^2|)^2/(N_{observed} - N_{parameters})]^{1/2}$.

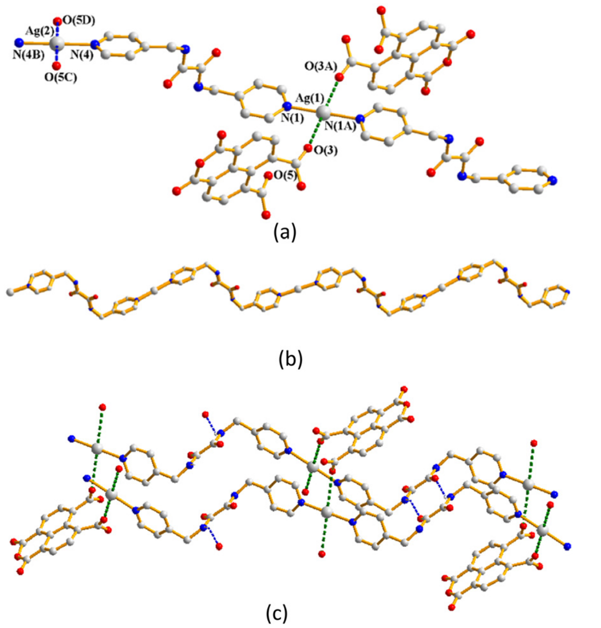

Fig. 3 (a) Coordination environments of Ag(I) cations in **1**. Symmetry transformations were used to generate equivalent atoms: (A) $-x + 2$, $-y$, $-z + 2$; (B) $-x + 1$, $-y$, $-z$; (C) x, y, $z - 1$; (D) $-x + 1$, $-y$, $-z + 1$. (b) A drawing showing the 1D zigzag chain. (c) A drawing showing the zigzag chains linked by the Ag⋯O interactions.

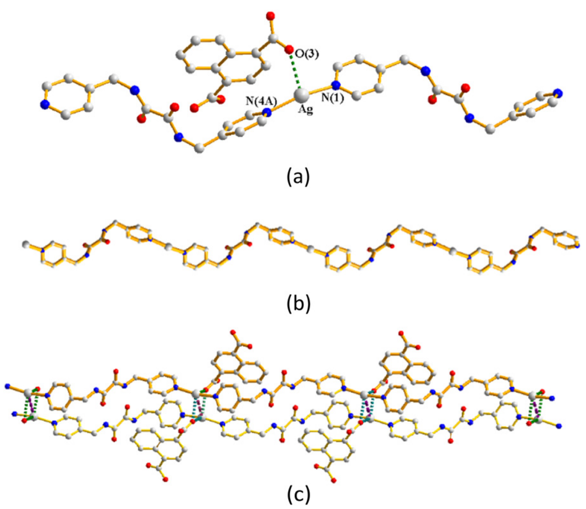

Fig. 4 (a) Coordination environment of the Ag(I) ion in **2**. Symmetry transformations were used to generate equivalent atoms: (A) x, $y - 1$, $z + 1$. (b) A drawing showing the 1D zigzag chain. (c) A drawing showing the double chain supported by the Ag⋯Ag and Ag⋯O interactions.

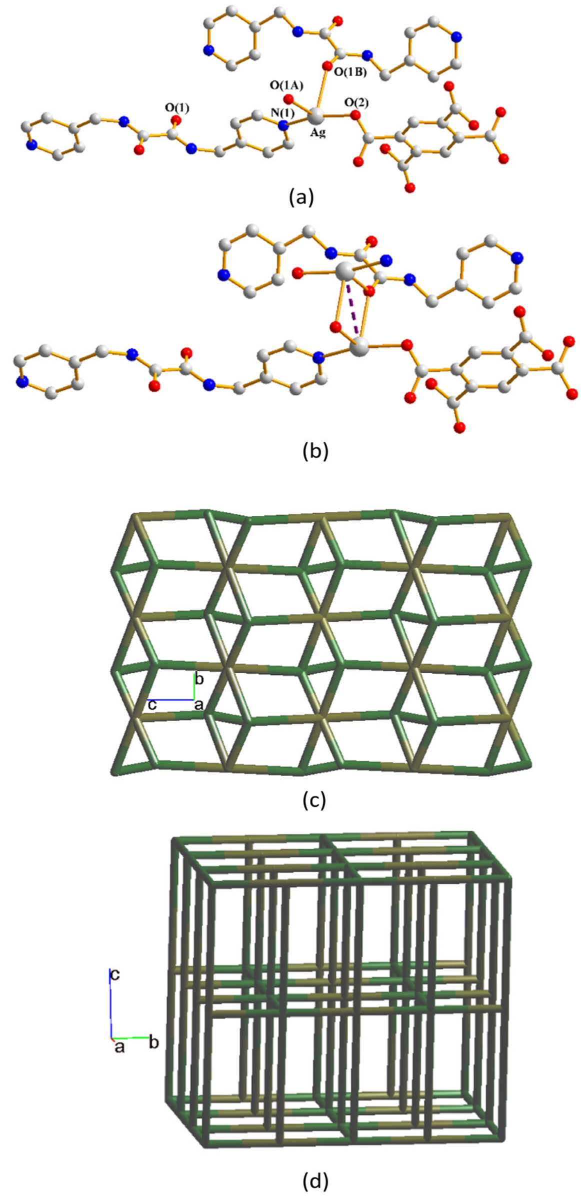

Fig. 5 (a) Coordination environment of the Ag(I) ion in **3**. Symmetry transformations were used to generate equivalent atoms: (A) $-x + 3/2$, $y - 1/2$, $-z + 1/2$. (B) $x - 1/2$, $-y + 3/2$, $z - 1/2$. (b) A drawing showing the dinuclear unit. (c) A drawing showing the **fsh** topology. (d) A drawing showing the **fsc** topology.

regarding the $\mathbf{L^1}$ ligand as 6-connected nodes and Ag(I) ions as 4-connected nodes, with the 1,2,4,5-H_2BTC^{2-} ligand as linkers, the structure can be simplified as a 4,6-connected 3D net with the $(4^3{\cdot}6^3)_2(4^6{\cdot}6^6{\cdot}8^3)$-**fsh** topology (standard representation) (Fig. 5(c)). Moreover, if the $\mathbf{L^1}$ ligands are considered as 4-connected nodes, and the dinuclear Ag(I) units as 6-connected nodes, with the 1,2,4,5-H_2BTC^{2-} ligand as linkers, the structure can be further simplified as a 4,6-connected 3D net with the $(4^4{\cdot}6^{10}{\cdot}8)(4^4{\cdot}6^2)$-**fsc** topology (cluster representation) (Fig. 5(d)), determined by using ToposPro.[31]

Structure of $\{[Ag(\mathbf{L^1})(H_2O)][1,2,4,5\text{-}H_3CTC]{\cdot}H_2O\}_n$, 4

Crystals of complex **4** conform to the monoclinic space group $P2_1/n$ and the asymmetric unit comprises one Ag(I) cation, one $\mathbf{L^1}$ ligand, one 1,2,4,5-H_3CTC^- ligand and two water molecules. One of the two water molecules interacts significantly with the Ag(I) cation [Ag⋯O = 2.584(2) Å]. The Ag(I) cation is two-coordinated by two pyridyl nitrogen atoms from two $\mathbf{L^1}$ ligands [Ag–N = 2.1395(16) and

2.1519(16) Å], resulting in a distorted linear geometry (Fig. 6(a)). If the Ag⋯O distance of 2.584(2) Å to the oxygen atom of the water molecule is regarded as a coordinate covalent bond, the Ag(I) cation may adopt a distorted triangular geometry. The Ag(I) cations are linked by the **L¹** ligands to form 1D zigzag chains (Fig. 6(b)). The 1D chains are supported by the Ag⋯Ag interactions [3.2002(5) Å] and N–H⋯O [O⋯H = 2.033(2); ∠N–H⋯O = 151.3(1)°] hydrogen bonds to form double chains (Fig. 6(c)), which are also supported by the Ag⋯O interactions [Ag⋯O = 2.687(2) Å] to the amide oxygen atoms of the other pair (Fig. 6(d)).

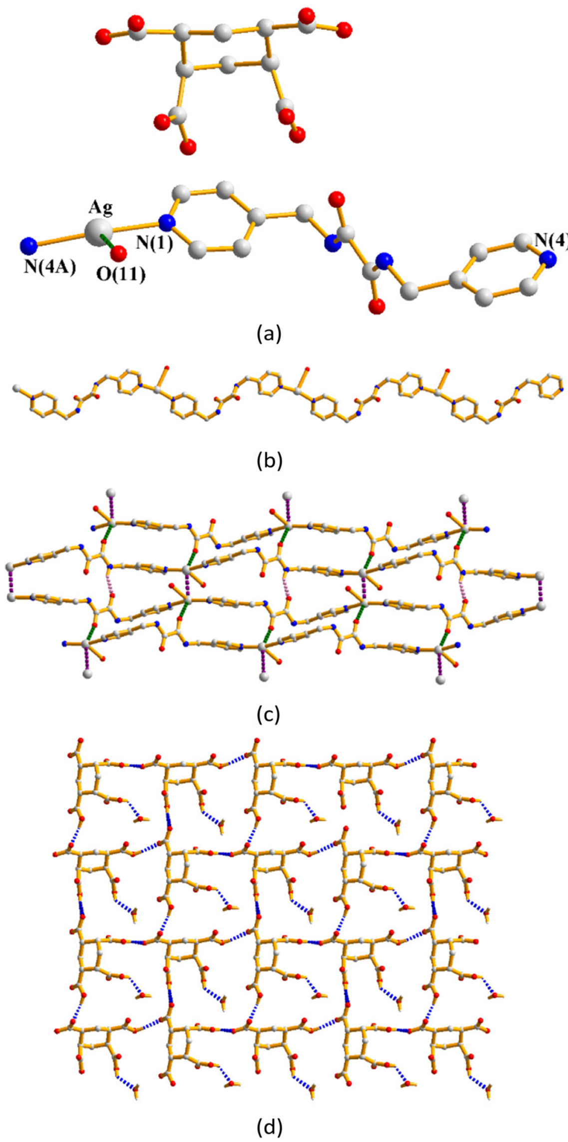

Fig. 6 (a) Coordination environment of the Ag(I) ion in **4**. Symmetry transformations were used to generate equivalent atoms: (A) $x + 1$, $y + 1$, z. (b) A drawing showing the 1D zigzag chain. (c) A drawing showing the double chains supported by the Ag⋯Ag and Ag⋯O interactions. (d) A drawing showing the 1,2,4,5-H_3CTC^- ligands linked through the O–H⋯O hydrogen bonds.

Structure of {[Ag(L^2)][1,4-HNDC]·H_2O}$_n$, 5

Complex **5** crystallizes in the monoclinic space group $P2_1/n$. The asymmetric unit consists of one Ag(I) cation, one **L²** ligand, one 1,4-$HNDC^-$ ligand and one cocrystallized water molecule. The Ag(I) cation is two-coordinated by two pyridyl nitrogen atoms from two **L²** ligands [Ag–N = 2.182(3) and 2.189(3) Å], resulting in a distorted linear geometry, while the anionic 1,4-$HNDC^-$ ligand interacts with the Ag(I) cation through the Ag⋯O interaction [Ag–O = 2.635(2) and 2.754(2) Å] (Fig. 7(a)). The Ag(I) cations are linked by the **L²** ligands to afford 1D zigzag chains (Fig. 7(b)). Moreover, the 1D zigzag chains are supported by extensive O–H⋯O hydrogen bonds, originating from the carboxylate hydrogen atoms to the carboxylate oxygen atoms [O⋯H = 1.695(2) Å; ∠O–H⋯O = 169.1(2)°] and from the water hydrogen atoms to the carboxylate oxygen atoms [O⋯H = 1.937(3) and 2.034(2) Å; ∠O–H⋯O = 171.8(2) and 169.1(2)°] (Fig. 7(c)).

Structure of {[$Ag_2(L^1)_2$][1,2,4-HBTC]·$2H_2O$}$_n$, 6

Crystals of complex **6** conform to the triclinic space group $P\bar{1}$. The asymmetric unit consists of two Ag(I) cations, two **L¹** ligands, one 1,2,4-$HBTC^{2-}$ ligand and two cocrystallized water molecules. The Ag(I) metal centers are two-coordinated by one nitrogen atom from two **L¹** ligands [Ag–N = 2.146(5) Å], resulting in a distorted linear geometry (Fig. 8(a)). The Ag(I) cations are linked by the **L¹** ligands to afford 1D zigzag chains (Fig. 8(b)). Moreover, the 1D zigzag chains are

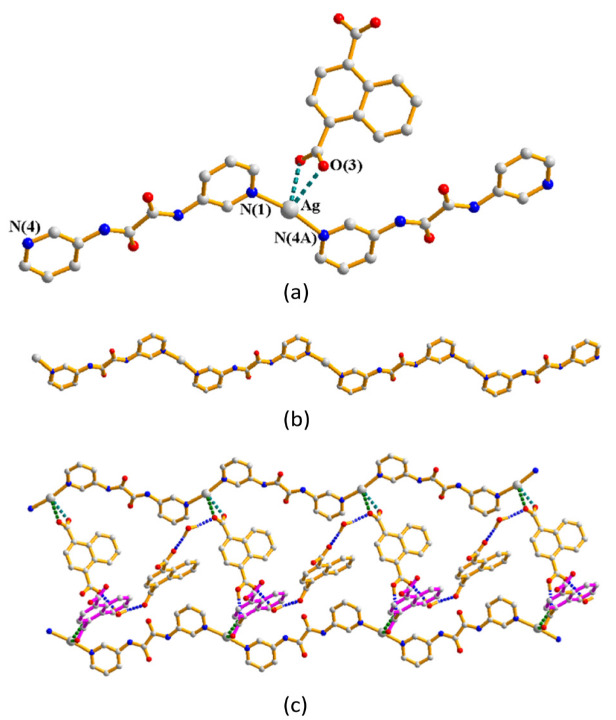

Fig. 7 (a) Coordination environment of the Ag(I) ion in **5**. Symmetry transformations used to generate equivalent atoms: (A) $x - 1$, y, $z + 1$. (b) A drawing showing the 1D zigzag chain. (c) A drawing showing the 1D zigzag chains supported by the O–H⋯O interactions.

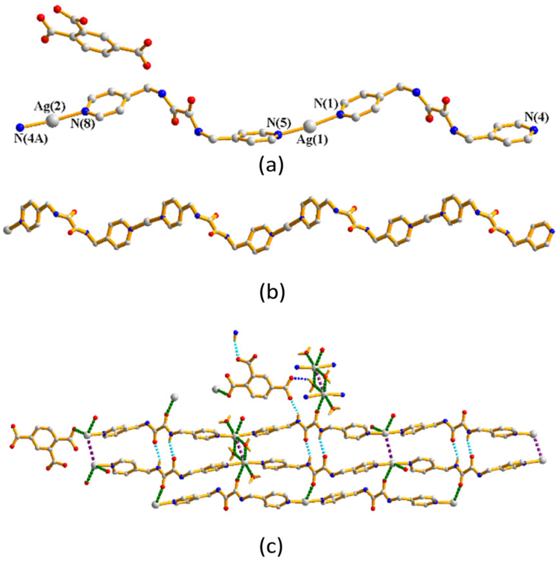

Fig. 8 (a) Coordination environment of Ag(I) ions in **6**. Symmetry transformations were used to generate equivalent atoms: (A) $x - 1$, $y + 2$, $z + 1$. (b) A drawing showing the 1D zigzag chain. (c) A drawing showing the double chain supported by the various interactions.

supported by the Ag⋯Ag interactions [Ag⋯Ag = 3.1054(10) and 3.5257(10) Å] and Ag⋯O interactions to the amide oxygen atoms [Ag⋯O = 2.862(4) and 3.096(4) Å], carboxylate oxygen atoms [Ag⋯O = 2.862(4) and 2.968(5) Å] and to the water oxygen atoms [Ag⋯O = 2.930(7), 2.884(5) and 3.049(5) Å]. Self-complementary N–H⋯O hydrogen bonds [O⋯H = 2.138(4) and 1.992(6) Å; ∠N–H⋯O = 149.9(4) and 147.8(4)°], N–H⋯O hydrogen bonds to the carboxylate oxygen atoms [O⋯H = 2.150(6) and 1.961(6) Å; ∠N–H⋯O = 162.1(4) and 146.5(4)°] and O–H⋯O hydrogen bonds [O⋯H = 2.096(6) Å; ∠O–H⋯O = 136.0(4)°] from the water molecules to the carboxylate oxygen atoms are also observed (Fig. 8(c)).

Structure of {[$Ag_2(\mathbf{L^1})_{1.5}$][(1,3,5-HBTC)(H_2O)]·$2H_2O$}$_n$, 7

The structure of complex **7** was solved in the triclinic space group $P\bar{1}$ and each asymmetric unit comprises two Ag(I) cations, one and a half $\mathbf{L^1}$ ligands, one 1,3,5-$HBTC^{2-}$ ligand, one coordinated water molecule and two co-crystallized water molecule. The Ag(1) atom is linked by two oxygen atoms from the 1,3,5-$HBTC^{2-}$ ligand [Ag–O = 2.176(4) Å] and water molecule [Ag–O = 2.534(5) Å] and one pyridyl nitrogen atom from the $\mathbf{L^1}$ ligand [Ag–N =2.175(6) Å]. Considering the Ag–O distance of 2.534(5) Å as a coordinate covalent bond, the Ag(1) atom adopts a distorted T-shaped geometry, whereas the Ag(2) metal center is three-coordinated by two oxygen atoms from the 1,3,5-$HBTC^{2-}$ ligand [Ag–O = 2.326(6) and 2.550(6) Å] and one pyridyl nitrogen atom from the $\mathbf{L^1}$ ligand [Ag–N =2.191(6) Å], resulting in a distorted triangular geometry. The Ag(I) ions are linked together by the 1,3,5-$HBTC^{2-}$ and $\mathbf{L^1}$ ligands to afford a linear tetranuclear molecule (Fig. 9(a)), which are linked by the O–H⋯N [H⋯N = 1.775(5) Å; ∠O–H⋯N = 166.1(3)°] hydrogen bonds from the

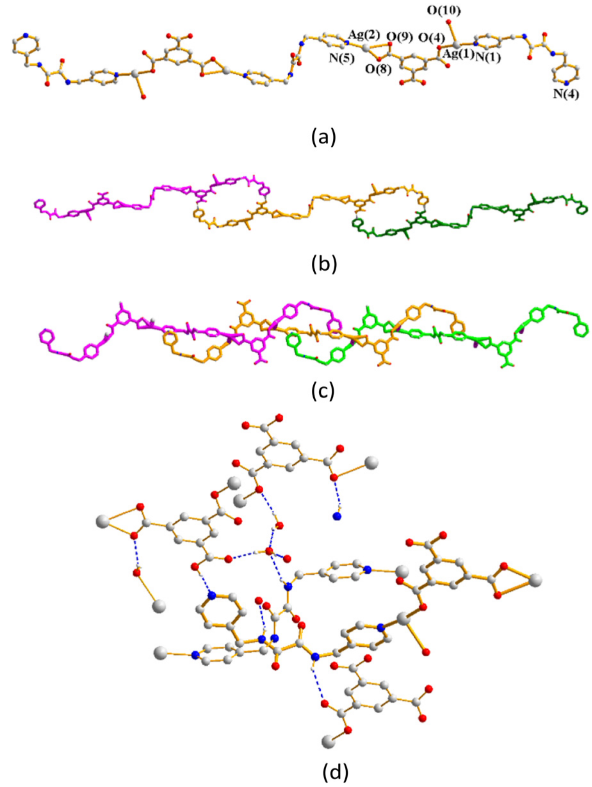

Fig. 9 (a) A drawing showing the tetranuclear structure of **7**. (b) A drawing showing the tetranuclear chain terminated by the O–H⋯N hydrogen bonds. (c) A drawing showing the interweaved chain of the tetranuclear molecules. (d) A drawing showing the hydrogen bonds that linked the molecules of **7**.

carboxylate hydrogen atom to N(4) that terminates the extension of the tetranuclear molecule. Moreover, the tetranuclear molecules are interweaved through the Ag⋯Ag interactions [Ag⋯Ag = 3.0190(8) Å] to form a 1D chain (Fig. 9(b)). The interweaved chains (Fig. 9(c)) are also supported by the N–H⋯O hydrogen bonds from the amine hydrogen atoms to the carboxylate oxygen atoms [H⋯O = 2.362(4) and 2.234(5) Å; ∠N–H⋯O = 131.3(3) and 155.1(4)°] and coordinated water molecules [H⋯O = 2.164(5) Å; ∠N–H⋯O = 152.9(4)°], as well as the O–H⋯O hydrogen bonds from the co-crystallized water molecules to the amide oxygen atoms [O⋯H = 1.984(5) Å; ∠O–H⋯O = 169.3(4)°] and the carboxylate oxygen atoms [O⋯H = 1.942(4), 2.033(4) and 2.026(5) Å; ∠O–H⋯O = 169.5(4), 145.1(4) and 138.3(4)°]. O–H⋯O hydrogen bonds between the co-crystallized water molecules are also observed [O⋯H = 2.100(5) Å; ∠O–H⋯O = 148.4(4)°] (Fig. 9(d)).

Crystal structure of {[$Ag(\mathbf{L^1})_{0.5}$][(1,3,5-H_2BTC)]}$_n$, 8

The structure of complex **8** was solved in the triclinic space group $P\bar{1}$ and each asymmetric unit comprises one Ag(I) cation, a half of an $\mathbf{L^1}$ ligand and one 1,3,5-H_2BTC^- ligand. The Ag(I) cation is three-coordinated by one oxygen atom from the 1,3,5-H_2BTC^- ligand [Ag–O = 2.164(1) Å], one pyridyl nitrogen atom from the **L**[1] ligand [Ag–N =2.182(1) Å], and one amide oxygen atom of the **L**[1] ligand [Ag–O = 2.584(2) Å], resulting in a distorted T-shaped geometry (Fig. 10(a)). Moreover, the structure is further extended through the Ag⋯Ag [Ag⋯Ag = 3.4378(8) Å] interactions and O–H⋯O hydrogen bonds originating from the carboxylate hydrogen atoms to the carboxylate oxygen atoms [O⋯H = 1.804(2) and 1.8388(14) Å; ∠O–H⋯O = 156.6(1)° and 174.8(1)°] (Fig. 10(b)). If the **L**[1] ligands are considered as four-coordinated nodes, and the Ag(I) ions as two coordinated nodes, the structure of complex **8** can be regarded as a 2,4-connected 1D net with the $(4^2)(4)_2$-2,4C4 topology (Fig. 10(c)).

Structure of {[Ag$_5$(1,3,5-HBTC)(1,3,5-BTC)(L^1)$_2$]·5H$_2$O}$_n$, 9

The structure of complex **9** was solved in the triclinic space group $P\bar{1}$ and each asymmetric unit comprises four and two halves of Ag(I) cations, two **L**[1] ligands, one 1,3,5-HBTC^{2-} ligand, one 1,3,5-BTC^{3-} ligand and five co-crystallized water molecules. While the Ag(1) and Ag(4) atoms form the distorted T-shaped geometries and the Ag(2) and Ag(5) atoms form the bent ones, Ag(3) and Ag(6) adopt linear geometries (Fig. 11(a)). The Ag(1) cation is three-coordinated by two oxygen atoms from the 1,3,5-HBTC^{2-} [Ag–O = 2.320(3) Å] and 1,3,5-BTC^{3-} ligands [Ag–O = 2.328(3) Å] and one pyridyl nitrogen atom from the **L**[1] ligand [Ag–N = 2.317(3) Å]. The

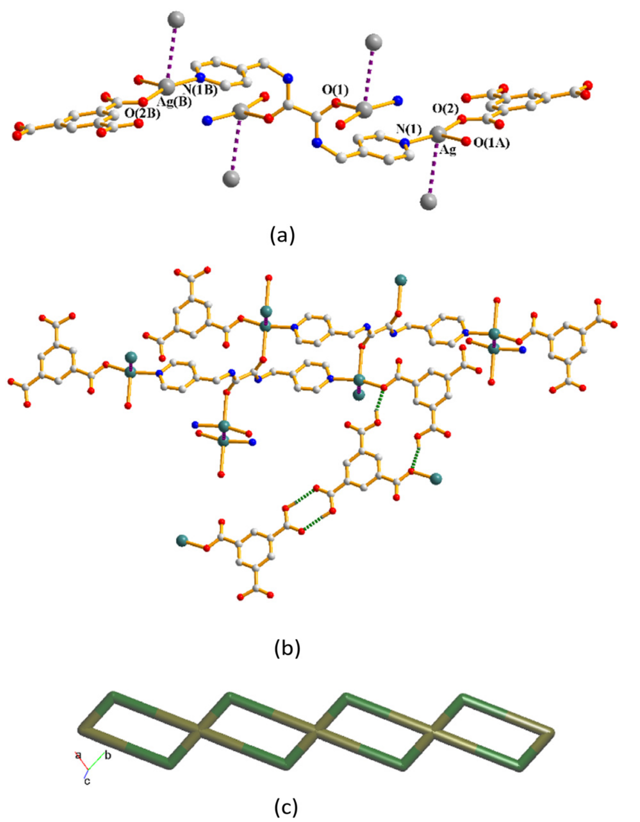

Fig. 10 (a) A drawing showing the coordination environments of the Ag(I) cations of **8**. (b) A drawing showing the Ag⋯Ag interactions and O–H⋯O hydrogen bonds. (c) A drawing showing the 2,4C4 topology.

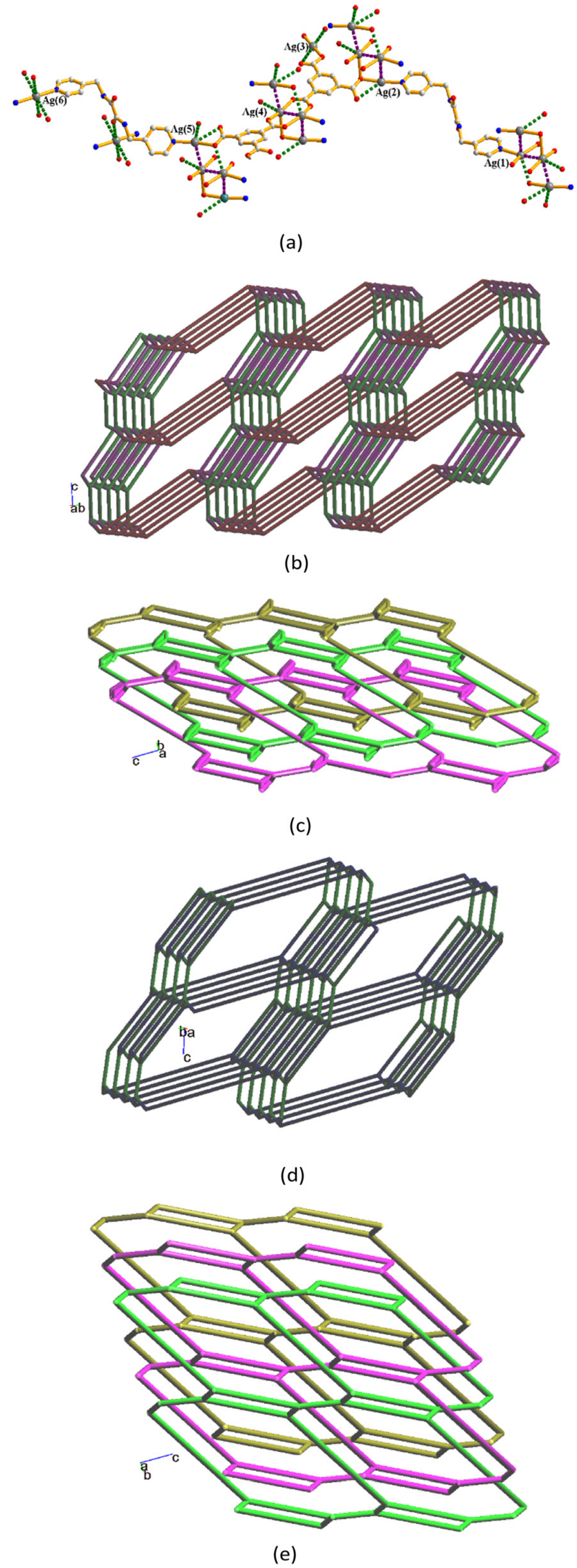

Fig. 11 (a) A drawing showing the coordination environments of the Ag(I) cations of **9**, as well as the Ag⋯Ag and Ag⋯O interactions. Symmetry transformations were used to generate equivalent atoms: (A) $x-1$, y, z. (B) $-x-2$, $-y+3$, $-z+1$. (b) A drawing showing the $(4{\cdot}10^2)(4{\cdot}6{\cdot}8)(4^2{\cdot}6^3{\cdot}8^3{\cdot}10^2)(4^2{\cdot}6)$ topology. (c) A drawing showing the 3-fold interpenetration. (d) A drawing showing the $(4^2{\cdot}6^3{\cdot}8)$-**sra** topology. (e) A drawing showing the 3-fold interpenetration with the **sra** topology.

Ag(2) cation is two-coordinated by one oxygen atom from the 1,3,5-BTC^{3-} [Ag–O = 2.136(3) Å] ligand and one pyridyl nitrogen atom from the $\mathbf{L^1}$ ligand [Ag–N = 2.138(3) Å]. The Ag(3) cation is two-coordinated by two symmetry-related oxygen atoms from the 1,3,5-BTC^{3-} [Ag–O = 2.190(3) Å] ligand. The Ag(4) cation is three-coordinated by three oxygen atoms from one 1,3,5-$HBTC^{2-}$ ligand [Ag–O = 2.171(3) Å] and two 1,3,5-BTC^{3-} ligands [Ag–O = 2.182(3) and 2.574(3) Å]. The Ag(5) cation is two-coordinated by one oxygen atom from the 1,3,5-$HBTC^{2-}$ [Ag–O = 2.182(3) Å] ligand and one pyridyl nitrogen atom from the $\mathbf{L^1}$ ligand [Ag–N = 2.169(3) Å]. The Ag(6) cation is two-coordinated by two symmetry-related nitrogen atoms from two $\mathbf{L^1}$ ligands [Ag–N = 2.227(3) Å].

The Ag(I) cations are interlinked through the Ag⋯Ag [Ag⋯Ag = 3.3661(22), 2.8959(16) and 3.0012(23) Å] and Ag⋯O interactions [Ag⋯O = 2.970(5), 2.749(4), 2.639(9), 2.910(5) and 2.963(4) Å] to form linear tetranuclear geometries, while the other Ag⋯O interactions [Ag⋯O = 2.799(4), 2.766(3) and 2.976(3) Å] that support the structure are also observed. Considering the Ag(1) and Ag(4) cations and 1,3,5-$HBTC^{2-}$ ligands as 3-connected nodes and 1,3,5-BTC^{3-} ligands as five-connected nodes, with the other Ag(I) cations and $\mathbf{L^1}$ ligands as linkers, the structure of **9** can be simplified as a 3,3,3,5-connected 3D net with the $(4{\cdot}10^2)(4{\cdot}6{\cdot}8)(4^2{\cdot}6^3{\cdot}8^3{\cdot}10^2)(4^2{\cdot}6)$ topology (standard representation) (Fig. 11(b)), showing 3-fold interpenetration (Fig. 11(c)). Moreover, if the 1,3,5-BTC^{3-} ligands and the bridged dinuclear Ag(I) units are considered as 4-connected nodes, the structure can be further simplified as a 4,4-connected 3D net with the $(4^2{\cdot}6^3{\cdot}8)$-sra topology (cluster representation) (Fig. 11(d)), revealing the 3-fold interpenetration (Fig. 11(e)).

Ag⋯Ag and Ag⋯O distances and structural types

Table 2 lists the Ag⋯Ag and Ag⋯O distances in complexes **1–9**, which demonstrate that these distances are subjected to the changes of the polycarboxylate anions. If the Ag⋯O distance for the coordinate covalent bond is set to be less than 2.6 Å, only complexes **3**, **4**, **7**, **8** and **9** show Ag–O coordinate covalent bonds, while the others adopt Ag⋯O interactions. On the basis of the coordinate covalent bonds involving Ag–N and Ag–O, complexes **1**, **2**, **4**, **5** and **6** form 1D zigzag chains, whereas complex **3** is a 3D framework with the **fsc** topology, **7** shows interweaved tetranuclear molecules, **8** displays a 1D chain with the 2,4C4 topology and **9** reveals a 3-fold interpenetrated 3D net with the sra topology. It is noted that the Ag⋯Ag distances are also subjected to the changes of the polycarboxylate ligands. The Ag⋯Ag interactions of these complexes except **3** are supported by the polycarboxylate ligands through the weak Ag⋯O interactions and hydrogen bonds, instead of the Ag–O coordinate covalent bonds, which can most probably be regarded as "ligand-unsupported". The Ag⋯Ag interaction of **3** is thus "ligand-supported".

Ligand conformations and bonding modes

The descriptor for assigning the ligand conformation is summarized pointwise: (1) based on the relative orientation of two C═O (or N–H) groups, on the same or opposite direction, the ligand can adopt *cis* or *trans* conformation. (2) Due to the relative orientation of the nitrogen atom on the pyridyl ring and the carbonyl group of amide, three more orientations, *anti–anti*, *syn–anti* and *syn–syn*, are possible for the ligand. Accordingly, the ligand conformations of $\mathbf{L^1}$ and $\mathbf{L^2}$ in complexes **1–9** are summarized in Table 3, in which complex **9** shows two independent $\mathbf{L^1}$ ligands with the same ligand conformation. While the $\mathbf{L^1}$ ligands in complexes **3** and **8** bridge six and four Ag(I) cations, respectively, through the pyridyl nitrogen and amide oxygen atoms, the ligands in the other complexes bridge two cations through the two pyridyl nitrogen atoms, considering the Ag⋯O distances less than 2.6 Å as the coordinate covalent bonds. Moreover, Table 4 gives the bonding modes of the polycarboxylate ligands. While those in complexes **1**, **2**, **4**, **5** and **6** show no Ag–O coordinate covalent bond, the others coordinate with one to five Ag(I) cations. Noticeably, the anions of 1,3,5-H_3BTC in **7–9** coordinate at least with one Ag(I) cation, probably indicating their better basicity than the other polycarboxylate ligands toward the Ag(I) cations.

Powder X-ray analysis

In order to check the phase purity of the products, powder X-ray diffraction (PXRD) experiments were carried out for

Table 2 Ag⋯Ag and Ag⋯O distances (Å) in complexes **1–9**

Complex	Ag⋯Ag	Ag⋯O
1		2.895(3) and 3.216(4) (P)
2	3.4832(8)	2.616(3) and 2.662(4) (P)
3	3.4763(7)	2.536(3) and 2.597(3) (A); 2.218(3) (P)
4	3.2002(5)	2.584(2) (W)
5		2.635(2) and 2.754(2) (P)
6	3.1054(10) and 3.5257(10)	2.862(4) and 3.096(4) (A); 2.862(4) and 2.968(5) (P); 2.930(7), 2.884(5) and 3.049(5) (W)
7	3.0190(8)	2.176(4), 2.326(6) and 2.550(6) (P); 2.534(5) (W)
8	3.4378(8)	2.164(1) (P); 2.584(2) (A)
9	3.3661(22), 2.8959(16) and 3.0012(23)	2.320(3), 2.328(3), 2.136(3), 2.190(3), 2.171(3), 2.182(3) 2.574(3), 2.910(5), 2.970(5), 2.749(4) and 2.976(3) (P); 2.639(9), 2.963(4) and 2.799(4) (W); 2.766(3) (A)

P: to the polycarboxylate oxygen atom; A: to the amide oxygen atom; W: to the water oxygen atom.

Table 3 Ligand conformations of L^1 and L^2 in **1–9**

1	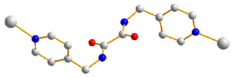 *Trans syn–syn*	**2**	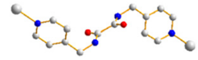 *Trans syn–syn*
3	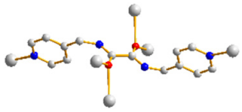 *Trans anti–anti*	**4**	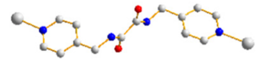 *Trans syn–anti*
5	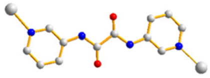 *Trans anti–anti*	**6**	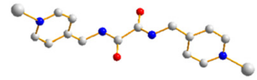 *Trans syn–anti*
7	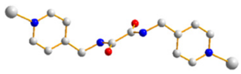 *Trans syn–anti*	**8**	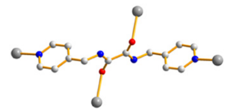 *Trans syn–syn*
9	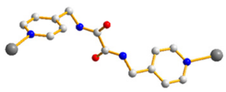 *Trans anti–anti*		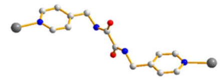 *Trans anti–anti*

Table 4 Bonding modes of the polycarboxylate ligands in **1–9**

1	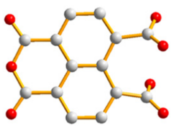	**2**	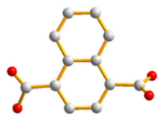
3	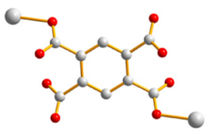	**4**	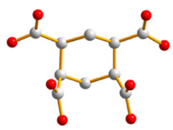
5	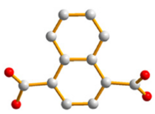	**6**	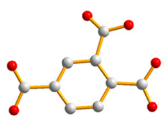
7	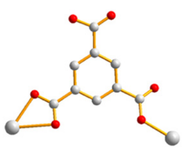	**8**	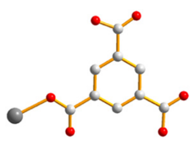
9	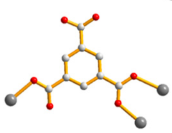		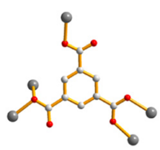

complexes **1–9**. As shown in Fig. S10–S18, the peak positions of the experimental and simulation PXRD patterns are in agreement with each other.

Conclusions

Eight bpba-based Ag(I) CPs and one tetranuclear molecule containing the polycarboxylate ligands have been successfully obtained. Their structural types are susceptible to the changes of the polycarboxylate ligands and reaction conditions. Complexes **7–9** represent unique examples that diverse structures of Ag(I) CPs constructed from $\mathbf{L^1}$ and 1,3,5-H_3BTC can be obtained by careful evaluation of their metal to ligand ratios. While complexes **3** and **7–9** show Ag–O coordinate covalent bonds, giving **3** a 3D framework with the **fsh** topology, **7** a linear tetranuclear molecule, **8** a 1D looped chain, and **9** a 3-fold interpenetrated 3D framework with the **sra** topology, respectively, the other complexes reveal Ag⋯O interactions, adopting 1D zigzag chains. The geometries of the Ag(I) cations and the structural types of these complexes are presumably subjected to the determination of a Ag–O bond, which is set to be less than 2.6 Å in this report. The identities of the polycarboxylate ligands are important in determining the strengths of the "ligand-unsupported" and "ligand-supported" Ag⋯Ag interactions in complexes **2–4** and **6–9** as well.

Author contributions

Investigation, Y.-L. S. and C.-L. L.; data curation, H.-C. T. and Z.-L. C.; review and supervision, J.-D. C. All authors have read and agreed to the published version of the manuscript.

Conflicts of interest

There are no conflicts to declare.

Data availability

The data supporting this article have been included as part of the SI.

Supplementary information: ORTEP drawings (Fig. S1–S9). PXRD patterns (Fig. S10–S18). See DOI: https://doi.org/10.1039/d5ce01151e.

CCDC 2512227–2512235 (**1**–**9**) contain the supplementary crystallographic data for this paper.[32a–i]

Acknowledgements

We are grateful to the National Science and Technology Council of the Republic of China for support.

References

1 W. P. Lustig, S. Mukherjee, N. D. Rudd, A. V. Desai, J. Li and S. K. Ghosh, *Chem. Soc. Rev.*, 2017, **46**, 3242–3285.

2 S. R. Batten, S. M. Neville and D. R. Turner, *Coordination Polymers Design, Analysis and Application*, The Royal Society of Chemistry, London, UK, 2009.

3 S. Mondal and P. Dastidar, *Cryst. Growth Des.*, 2020, **20**, 7411–7420.

4 V. Chandrasekhar, C. Mohapatra, R. Banerjee and A. Mallick, *Inorg. Chem.*, 2013, **52**, 3579–3581.

5 J. Yu, Y. Cheng, X. Zhang, L. Zhou, Z. Song, A. Nezamzadeh-Ejhieh and Y. Huang, *J. Environ. Chem. Eng.*, 2025, **13**, 116870.

6 P. Yan, Z. Chen, X. Li, F. Liang, Y. Tan, Y. Lin, K. Yang, C. Xiao, J. Wu and D. Ma, *J. Solid State Chem.*, 2024, **330**, 124461.

7 F. Liang, D. Ma, L. Qin, Q. Yu, J. Chen, R. Liang, C. Zhong, H. Liao and Z. Peng, *Dalton Trans.*, 2024, **53**, 10070–10074.

8 Y. Zhang, H. Tan, J. Zhu, L. Duan, Y. Ding, F. Liang, Y. Li, X. Peng, R. Jiang, J. Yu, J. Fan, Y. Chen, R. Chen and D. Ma, *Molecules*, 2024, **29**, 5903.

9 S. Li, J. Sun, G. Liu, S. Zhang, Z. Zhang and X. Wang, *Chin. Chem. Lett.*, 2024, **35**, 109148.

10 Y. Ma, L. Yang, X. Bai and K. Wang, *Spectrochim. Acta, Part A*, 2025, **341**, 126471.

11 D. Ma, T. Liang, J. Zheng, G. Chen, Y. Ye, A. Nezamzadeh-Ejhieh, L. Lu, Z. Song and Y. Huang, *React. Funct. Polym.*, 2026, **218**, 106520.

12 V. Lakshmanan, Y.-T. Lai, X.-K. Yang, M. Govindaraj, C.-H. Lin and J.-D. Chen, *Polymer*, 2021, **13**, 3018.

13 W.-T. Lee, T.-T. Liao and J.-D. Chen, *Int. J. Mol. Sci.*, 2022, **23**, 3603.

14 V. Lakshmanan, C.-Y. Lee, Y.-W. Tseng, Y.-H. Liu, C.-H. Lin and J.-D. Chen, *CrystEngComm*, 2022, **24**, 6076–6086.

15 J. L. Sague, M. Meuwly and K. M. Fromm, *CrystEngComm*, 2008, **10**, 1542–1549.

16 Y.-C. He, X.-H. Li, Y.-M. Ruan, Q. Xu, S.-X. Li, H.-X. Mao, F.-H. Zhao and M.-T. Li, *Inorg. Chim. Acta*, 2023, **557**, 121710.

17 Y.-H. Li, D. Sun, G.-G. Luo, F.-J. Liu, H.-J. Hao, Y.-M. Wen and Y. Zhao, *J. Mol. Struct.*, 2011, **1000**, 85–91.

18 Y. Li a, C. Xiao, S. Li, Q. Chen, B. Li, Q. Liao and J. Niu, *J. Solid State Chem.*, 2013, **200**, 251–257.

19 V. Moodley, L. Mthethwa, M. N. Pillay, B. Omondi and W. E. van Zyl, *Polyhedron*, 2015, **99**, 87–95.

20 O. Z. Yeşilel, G. Günay, C. Darcan, M. S. Soylu, S. Keskin and S. W. Ng, *CrystEngComm*, 2012, **14**, 2817–2825.

21 A. Stephenson and M. D. Ward, *RSC Adv.*, 2012, **2**, 10844–10853.

22 H.-Y. Shi, Y.-B. Dong, Y.-Y. Liu and J.-F. Ma, *CrystEngComm*, 2014, **16**, 5110–5120.

23 Z. Ma, X. Song, Z. Li, Y. Ren, J. Wang and Y. Liang, *Dalton Trans.*, 2024, **53**, 3797–3807.

24 S. Kintzel, K. Eckhardt, J. Getzschmann, V. Bon, J. Grothe and S. Kaskel, *Eur. J. Inorg. Chem.*, 2020, 3167–3173.

25 K. Singh, J. R. Long and P. Stavropoulos, *J. Am. Chem. Soc.*, 1997, **119**, 2942–2943.

26 S. Muthu, J. H. K. Yip and J. J. Vittal, *J. Chem. Soc., Dalton Trans.*, 2002, 4561–4568.

27 A. Bondi, *J. Phys. Chem.*, 1964, **68**, 441–451.

28 K. B. Thapa and J.-D. Chen, *CrystEngComm*, 2015, **17**, 4611–4626.

29 Bruker AXS, *APEX2, V2008.6, SADABS V2008/1, SAINT V7.60A, SHELXTL V6.14*, Bruker AXS Inc., Madison, WI, USA, 2008.

30 G. M. Sheldrick, *Acta Crystallogr., Sect. A:Found. Crystallogr.*, 2008, **64**, 112–122.

31 V. A. Blatov, A. P. Shevchenko and D. M. Proserpio, *Cryst. Growth Des.*, 2014, **14**, 3576–3586.

32 (*a*) CCDC 2512227: Experimental Crystal Structure Determination, 2025, DOI: 10.5517/ccdc.csd.cc2qb5lv; (*b*) CCDC 2512228: Experimental Crystal Structure Determination, 2025, DOI: 10.5517/ccdc.csd.cc2qb5mw; (*c*) CCDC 2512229: Experimental Crystal Structure Determination, 2025, DOI: 10.5517/ccdc.csd.cc2qb5nx; (*d*) CCDC 2512230: Experimental Crystal Structure Determination, 2025, DOI: 10.5517/ccdc.csd.cc2qb5py; (*e*) CCDC 2512231: Experimental Crystal Structure Determination, 2025, DOI: 10.5517/ccdc.csd.cc2qb5qz; (*f*) CCDC 2512232: Experimental Crystal Structure Determination, 2025, DOI: 10.5517/ccdc.csd.cc2qb5r0; (*g*) CCDC 2512233: Experimental Crystal Structure Determination, 2025, DOI: 10.5517/ccdc.csd.cc2qb5s1; (*h*) CCDC 2512234: Experimental Crystal Structure Determination, 2025, DOI: 10.5517/ccdc.csd.cc2qb5t2; (*i*) CCDC 2512235: Experimental Crystal Structure Determination, 2025, DOI: 10.5517/ccdc.csd.cc2qb5v3.